Trees
DOI 10.1007/s00468-016-1366-9

ORIGINAL ARTICLE

Dense Canopy Height Model from a low-cost photogrammetric platform and LiDAR data

Mónica Herrero-Huerta[1] · Beatriz Felipe-García[2] · Soledad Belmar-Lizarán[3] · David Hernández-López[3] · Pablo Rodríguez-Gonzálvez[1] · Diego González-Aguilera[1]

Received: 5 January 2015 / Accepted: 15 February 2016

Abstract
Key message **Low-cost methodology to obtain CHMs integrating terrain data from LiDAR into photogrammetric point clouds with greater spatial, radiometric and temporal resolution due to a correction model.**
Abstract This study focuses on developing a methodology to generate a Dense Canopy Height Model based on the registration of point clouds from LiDAR open data and the photogrammetric output from a low-cost flight. To minimise georeferencing errors from dataset registration, terrain data from LiDAR were refined to be included in the photogrammetric point cloud through a correction model supported by a statistical analysis of heights. As a result, a fusion point cloud was obtained, which applies LiDAR to characterize the terrain in areas with high vegetation and utilizes the greater spatial, radiometric and temporal resolution of photogrammetry. The obtained results have been successfully validated: the accuracy of the fusion cloud is statistically consistent with the accuracies of both clouds based on the principles of classical photogrammetry and LiDAR processing. The resulting point cloud, through a radiometric and geometric segmentation process, allows a Dense Canopy Height Model to be obtained.

Keywords Dense Canopy Height Model · Photogrammetry · LiDAR · Data fusion · Low-cost platform · Radiometric segmentation

Communicated by E. Priesack.

✉ Mónica Herrero-Huerta
monicaherrero@usal.es

[1] Department of Cartographic and Land Engineering, Higher Polytechnic School of Avila, University of Salamanca, Hornos Caleros 50, 05003 Ávila, Spain

[2] Forestry and Natural Spaces Service, Agriculture, Environment and Rural Development Department, Castilla-La Mancha Regional Government, C/Mayor 46, 02001 Albacete, Spain

[3] Institute for Regional Development (IDR), University of Castilla La Mancha, 02071 Albacete, Spain

Introduction

The estimation of dasometric variables of interest for forest management (diameter, height, basal area, volume of growing stock, biomass, species, etc.) has traditionally been done via pilot samplings of field inventories. The advent of new remote sensing technologies and photogrammetry has opened up a new field of possibilities for carrying out such work, and such methods are advantageous in the economic costs involved, the time invested and estimation errors.

The application of active high-resolution remote sensors affords high accuracy in height measurements and a good prediction of dasometric variables (Popescu et al. 2002). In particular, the capacity of active light detection and ranging (LiDAR) sensors to penetrate and acquire three-dimensional measurements of the canopy at different heights (Wulder et al. 2013) allows improved estimation of variables such as biomass, volume and basal area over that of other sensors that gather two-dimensional data, such as photographic or radiometric systems. Since the late 1980s, studies have been published based on profiles acquired using airborne laser systems (ALS—airborne laser scanner) for the estimation of biomass and volumes (Nelson et al. 1988) as well as simple and multiple linear models (Nelson et al. 1997; Means et al. 2000) to analyse the effect of the lag transformation of the forest variable. Later studies

Published online: 25 February 2016

(Naesset 1997; Nelson et al. 2003) have improved upon studies of forest inventories by further exploiting instrumentation, capture methodology and information processing. Of interest are the studies of Lim and Treitz (2004) and Naesset (2004), in which the authors applied rodal[1] methods to generate inventories, as well as individual tree methods,[2] in which methodological compendia are described with the algorithms used in each estimation. Comparisons of different LiDAR inventories (Naesset et al. 2005) and of photointerpretation and LiDAR (Eid et al. 2004) have been published.

In recent years, many studies and methodological review articles have been published describing the operating capacity and definitive implementation of LiDAR technology in the context of the extraction of forest variables (Hyyppä et al. 2008; Wulder et al. 2012; Kankare et al. 2013). Benko and Balenovic (2011) reported new experiences in inventory tasks and forest management in different environments, with an analysis of the accuracies achieved. Richardson and Moskal (2011) established classifications of vegetation via tree height and density. Another interesting case is the guide produced by the Canadian Forest Service as a current reference document based on all previously published studies. The guide provides a series of recommendations for inventorying forest applications based on rodal methods using LiDAR data (White et al. 2013a). Gleason and Im (2012) applied different automated learning approaches to estimate biomass in forests from aerial LiDAR data. The FullWave airborne LiDAR systems provide large bodies of information about the overall plant and forest structure in great detail (Weinacker et al. 2004; Mallet and Bretar 2009). However, the complex and tedious processing involved and the costs of such technology are definite drawbacks (Chauve et al. 2007; Gupta et al. 2010).

Magnussen et al. (2007) used Landsat satellite images to create inventories according to the spatial resolution factor. Similarly, LiDAR techniques have been applied to images captured by different remote sensing systems (Magnussen et al. 2000; Wulder et al. 2008a, b; Willers et al. 2012; Mora et al. 2013) and by traditional photogrammetry (Magnusson et al. 2007).

Within the framework of the National Aerial Orthoimage Plan, low-density (0.5 points/m^2) LiDAR sensor flights have been performed since 2008 throughout the Spanish territory. Thus, in recent years, different forest research teams have tested different applications using data from this source (Estornell et al. 2012; González-Ferreiro et al. 2014; Gonzalez et al. 2012; Navarro-Cerrillo et al. 2014). The problem with these mass data acquisitions is that they are very costly, their resolution is low, and they are implemented individually at a given moment in time.

Currently, conventional photogrammetry is a complementary alternative to custom LiDAR flights to obtain 3D-point clouds and digital surface models (DSMs) because the associated costs are lower (Järnstedt et al. 2012); the accuracy is greater; and the spatial, radiometric and temporal resolution is greater (Bohlin et al. 2012). The complementary nature of the two techniques can be seen in the greater planimetric accuracy of photogrammetry than LiDAR and the greater altimetric accuracy of the latter than of the former. Nevertheless, photogrammetry is incapable of generating a Digital Terrain Model (DTM) in zones covered by vegetation, and LiDAR information must be used to generate reference surfaces for the collection of vegetation heights (Järnstedt et al. 2012). As an advantage of the photogrammetric point cloud, White et al. (2013b) cite the ability to interpret species composition as well as the maturity and health of vegetation.

With the development of manned and unmanned low-cost aerial platforms (RPAS—Remotely Piloted Aircraft Systems), conventional photogrammetric data collection and analysis can still be performed. Tao et al. (2011) used dense photogrammetric point clouds obtained with RPAS over forested areas and obtained information about the tree density, its composition and changes in the forest canopy. Other authors (Jaakkola et al. 2010; Wallace et al. 2012) have combined cameras and light LiDAR systems on RPAS, thus allowing both sensors to be used at the same time. Finally, special attention should be paid to the study of Lisein et al. (2013), in which the authors generated a Canopy Height Model (CHM) of a hybrid nature, combining the DSM obtained by correlating images from a non-metric camera and an RPAS with a DTM obtained from ALS data to estimate different forest parameters.

The aim of the present work was to develop a low-cost, efficient and precise methodology to obtain CHMs destined for forest inventories such a stratification of forest masses or a stock calculation and for fire studies obtaining combustible models. This was achieved by integrating LiDAR terrain data with minor temporal variability, which are freely available from the National Geographic Institute of Spain, into photogrammetric point clouds obtained using a low-cost platform, for a desired area and time. Thus, we combined LiDAR's terrain-sensing capacity in densely vegetated zones with the greater spatial, radiometric and temporal resolution offered by low-cost photogrammetry in plant cover zones. A correction model was constructed for the two data sources to minimise the georeferencing errors produced by the low-cost photogrammetric process, thereby obtaining a registration accuracy in agreement with the accuracies of

[1] Rodal method: methods applied to a surface with similar arboreal characteristics.

[2] Individual-tree methods: methods applied differentially to each tree.

the point clouds generated by the two techniques. During data analysis, following the recommendations of Wang et al. (2007), we also incorporated a supervised classification of the vegetation based on image colour that allows morphological classification types to be improved. The low-cost photogrammetric platform we used was a powered paraglider trike, designed and developed by the Institute for Regional Development of the University of Castilla-La Mancha. The greatest advantage offered by this type of manned platform is its flexibility of flight, autonomy and payload capacity, allowing data acquisition over an extensive area using multiple sensors to be integrated without constraints on time, weight or volume.

Materials and methods

The proposed methodology uses LiDAR open data freely available from the National Geographic Institute of Spain (IGN 2015) with a spatial resolution of 0.5 points/m^2. The aerial LiDAR data were revised by visual inspection and later by manual refinement, correcting errors in the initial automatic classification and thus obtaining well-coded terrain points. To assess the quality of the classification, the initial and filtered data were contrasted by means of a confusion matrix (Kohavi and Provost 1998).

According to the technical specifications of the National Aerial Orthoimage Plan (CNIG 2009), based on the type of terrain and the vegetation, an altimetric accuracy of 0.40 m was established.

Equipment

The following equipment was employed for photogrammetric data acquisition:

- A Leica System 1200 GNSS-RTK device was used for surveying control and check points, with a relative and absolute precision better than 0.03 and 0.05 m, respectively.
- A compact Olympus EP-1 camera, the first camera which meets the design standards of the micro four thirds (MFT) system. Its main features are shown in Table 1.
- A manned aerial platform supported by a powered paraglider (PPG) trike built by Airges (Fig. 1) was used (Ortega-Terol et al. 2014). Its technical specifications are shown in Table 2. The Olympus EP-1 camera was installed aboard the PPG trike using an auto-stabilised mounting platform. The potential benefits of this low-cost system are evident: a payload capacity that allows the system to be loaded with a large number of sensors that could be used for multispectral studies; the

Table 1 Technical specifications of the photographic sensor

Olympus EP1	
Type	CMOS
Sensor size (max. resolution)	4032 × 3024 pixels
Sensor size	17.3 × 13 mm
Pixel size (sensor geometric resolution)	0.0043 mm
Focal length	17 mm
Total pixels	12.3 MPixel
Aperture	*f*/2.8

Fig. 1 Aerial photogrammetric platform (PPG trike) with the gimbal shown (*white rectangle*)

Table 2 Technical specifications of the manned aerial platform: PPG trike

Parameter	Value
Empty weight	110 kg
Maximum load	220 kg
Autonomy	3.5 h
Maximum speed	60 km/h
Motor	Rotax 503
Tandem paraglide	MACPARA Pasha 4
Emergency system	Ballistic Parachutes GRS 350
Gimbal	Stabilized with 2 degrees of freedom
Minimum sink rate	1.1
Maximum glide	8.6
Plant surface	42.23 m^2
Projected area	37.8 m^2
Wingspan	15.03 m
Plant elongation	5.35
Central string	3.51 m
Boxes	54
Zoom factor	100 %

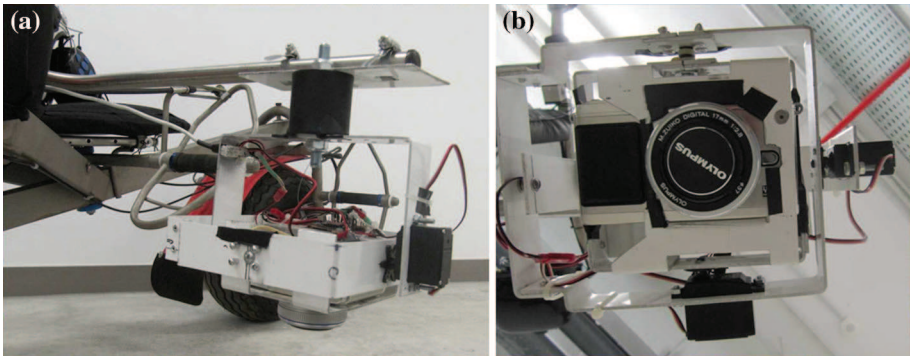

Fig. 2 Gimbal platform (auto-stabilised mounting platform). **a** Elevation view and **b** plan view

flexibility and autonomy of flying that offers the data acquisition over extensive areas.

- The PPG was equipped with a low-cost multi-sensor gimbal (stabilised platform), supporting the digital camera. The gimbal includes two servomotors oriented on the *x* and *y* axes to accurately maintain the camera's vertical position along the flight paths. The servomotors are controlled by an Arduino board, which incorporates an IMU with 6 degrees of freedom: three accelerometers with a range of ± 3.6 G m/s^2, a double-shaft gyroscope (for pitch and roll) and an additional gyroscope for yaw (both gyroscopes have a measurement range of ± 300°/s). The software developed to control the device is based on Quadl_mini V 20 software, with DCM (Direction Cosine Matrix) as the IMU management algorithm (Premerlani and Bizard 2014). Figure 2 shows the gimbal platform.
- The system included a low-cost GNSS system based on a single-frequency receptor, receiving signals from a GPS constellation and Satellite Based Augmentation System (SBAS) (NavCen 2008). The GNSS antenna is installed on the camera platform close to the optical centre of the camera to minimise the baseline. To improve the GNSS altitudinal accuracy, which affects the final GSD, a DigiFly VL100 barometer was installed. Thus, horizontal positioning during flight was performed using the GNSS system's National Marine Electronics Association (NMEA) protocol using RTKNAVI software (Takasu 2009), with corrections from the ground from similar equipment, allowing DGPS accuracies higher than 1.50 m in planimetry and 2 m in altimetry to be achieved in real time as well as accuracies higher than 0.50 m in three dimensions in post-processing.

Flight planning and execution

Proper flight planning is important to ensure that the captured photogrammetric data will fit the desired theoretical parameters; planning also optimises available resources and ensures higher quality images, minimising capture time. Flight planning was conducted with software developed by the IDR (Institute of Regional Development of Castilla-La Mancha, Spain), called PFlip, utilising fundamentals of photogrammetry, the sensor configuration, and the Digital Terrain Model (Hernández-López et al. 2013).

First, the study area was defined, followed by the flight strips. Furthermore, additional constraints such as a minimum forward overlap of 70 % and a minimum side overlap of 30 % were established to ensure automatic detection of tie points (Järnstedt et al. 2012). Then, the flight planning process defined the position and orientation of the camera, the design of different blocks of images, the overlaps between different images, the necessary shot angles and the scale, as defined by the choice of pixel size on the ground (GSD).

The geomatic information required for the flight planning process was obtained at no cost from the National Center of Geographic Information in Spain (CNIG 2015), from its National Aerial Orthoimage Plan, with a GSD of 0.25 m and a Digital Terrain Model with a 5-m grid resolution.

Flight planning was performed by considering the relationship among the flight height over the ground (H), the GSD, the focal length of the sensor (f) and the pixel size, as described in Eq. (1).

$$\frac{f}{H} = \frac{\text{pixel size}}{\text{GSD}} \tag{1}$$

Considering Eq. (1), the characteristics of the camera (Table 1) and the required GSD of 0.08 m, a flight height over the ground of 316 m was obtained. Based on the technical specifications of the National Aerial Orthoimage Plan (CNIG 2009), an 'a priori' altimetric accuracy of 0.10 m was estimated for the photogrammetric cloud.

The parameters that define image capture are determined during flight execution depending on the light conditions, the camera quality and flight speed. Thus, the camera configuration was established with a camera-

shooting interval of 4 s and a maximum flight speed of 14 m/s, which guaranteed a forward overlap of 70 %. A shutter speed of 1/1000 s was adequate for this speed because the equivalent terrain displacement would be 0.01 m, which was lower than 1/5 pixel, an insignificant value for study purposes. An ISO of 125 was used with a fixed focal length at infinity.

A topographic survey campaign was established to obtain absolute georeferencing and a model scaled through artificial accuracy targets. Targets were distributed along the study area so that they remained visible through vegetation for photogrammetric capture. Moreover, these targets were marked and their size confirmed to rule out effects from neighbouring pixels (35 cm diameter).

Photogrammetric processing

Low-cost photogrammetric workflow

Once the aerial imagery had been acquired, conventional photogrammetric processing began, relying on an image-based modelling technique. In an attempt to guarantee automation and quality, a combination of photogrammetric and computer vision algorithms was required. This approach allows data to be acquired remotely with great efficiency and accuracy, affording radiometric characteristics to the point cloud. Photogrammetry Workbench software (PW) developed by the authors (González-Aguilera et al. 2013) was used for three steps. First, the images were matched by the SIFT algorithm (Lowe 2004), which allowed the detection of the scene's points of interest. Second, the camera orientations were computed using the tie-points calculated in the previous step and the coordinates of the artificial ground targets located in the flight area (Pierrot-Deseilligny and Clery 2011). In this process, the external camera parameters (position and orientation) and the internal camera parameters were solved by self-calibration. Finally, a textured point cloud was obtained by means of ray intersection (Kraus 2007). To solve this process, an semi-global matching (SGM) technique (Pierrot-Deseilligny and Clery 2011) was applied.

Photogrammetric point cloud processing

Owing to the massive and automated nature of the photogrammetric point cloud, it was necessary to treat the cloud to remove outliers and encode the information. More precisely, a clean-up and classification process was used; this approach is schematised in Fig. 3. After removing the outliers produced by matching, the vegetation was distinguished via radiometric segmentation. Following this step, we established geometric classification of the "non-vegetation" class to differentiate it from "ground", refining the results via a second iteration. Once the uncertain points in the "ground" class and the isolated terrain points had been removed, we classified the other points into different semantic categories using the Axelsson algorithm (1999): "ground", "low vegetation", "medium vegetation", "high vegetation", "building" and "noise", according to the American Society for Photogrammetry and Remote Sensing (ASPRS Foundation 2012). During this process, special emphasis was placed on the classification of the "ground" class so that it would act as a common reference point for later collection of LiDAR and photogrammetric data. Additionally, it is crucial to achieve a correct DTM to obtain an accurate CHM.

Radiometric classification takes advantage of the RGB values of the photogrammetric point cloud. This step was carried out using in-house "Vegetation classification by radiometry" software. The analysis is based on the percentage differences between the digital levels of two channel pairs (R-G and R-B). Points were classified automatically according to a threshold defined by the difference from a green reference value. However, the values of green hues depend on many factors, such as the sensor employed, the conditions and date of flight, the type of species, the phenological state of the vegetation, etc. Accordingly, it is necessary to establish a threshold value from vegetation samples in the photogrammetric model.

Once the LiDAR information was corrected and the photogrammetric point cloud had been classified and refined, the point clouds were fused as described in the following section.

Fusion of point clouds

Before registering the point clouds, the ground photogrammetric points were filtered by cross-analysis with the LiDAR data to address errors caused in the classification process. To do so, we obtained a map of altimetric differences in ground-class zones shared between the two clouds. The photogrammetric points with large differences in height were reclassified as vegetation. We then generated a mask of the ground-class photogrammetric points to remove clusters of isolated points ($S < 2$ m^2) and the points contained within polygons with a high mean altimetric difference ($h > 1$ m). This filtering process allowed us to refine the terrain's photogrammetric data. Figure 4 shows the process used.

Low-cost photogrammetry includes georeferencing errors produced by the use of inertial sensors and low-accuracy GNSS and non-metric cameras. Accordingly, we designed a *correction model* to integrate the collected LiDAR data into the refined photogrammetric cloud, achieving a registration accuracy that was statistically compatible with the accuracy of both techniques. To

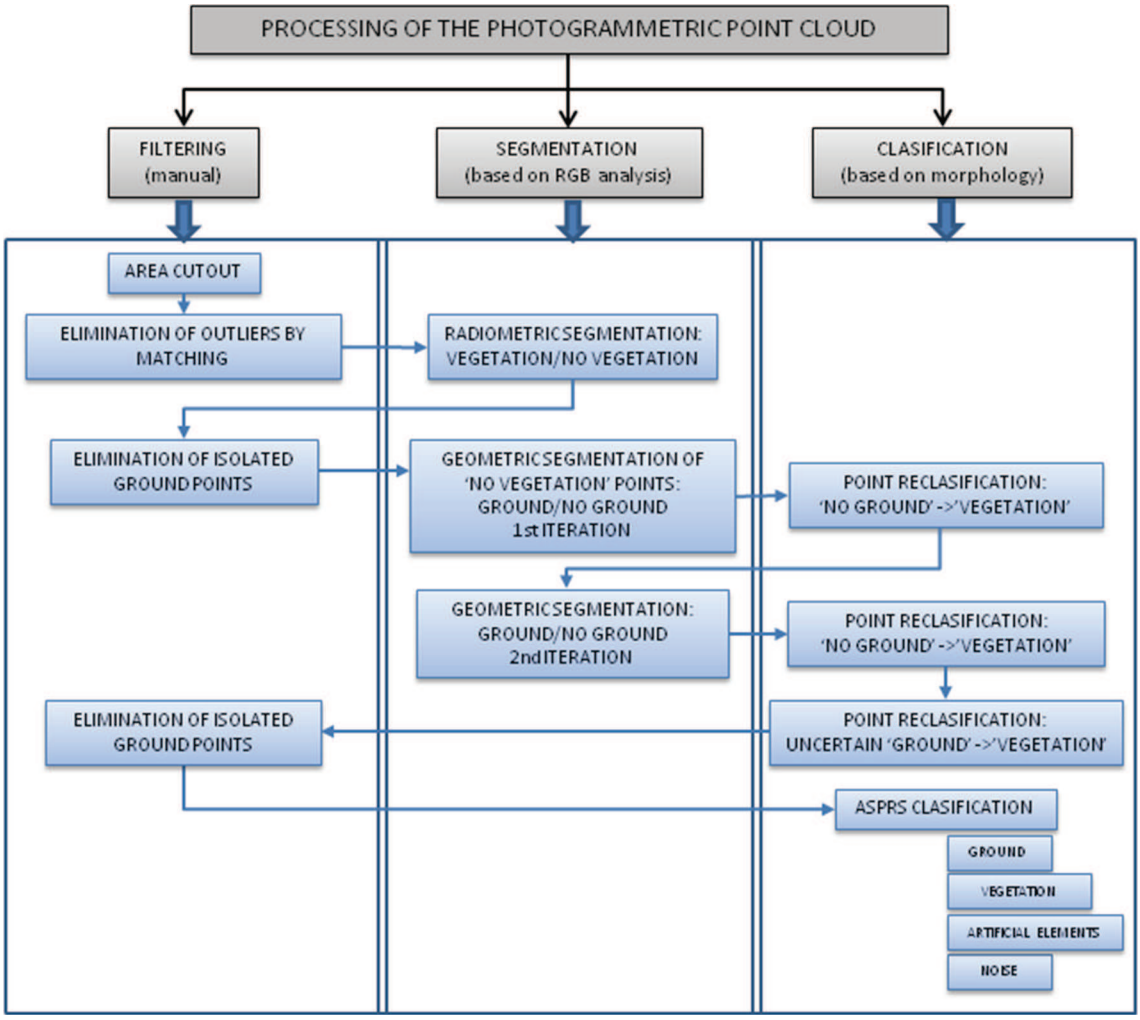

Fig. 3 Workflow for the processing and classification of the photogrammetric point cloud

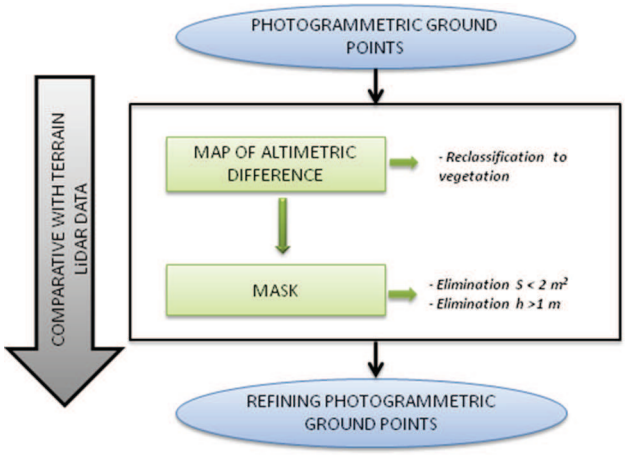

Fig. 4 Refining of the photogrammetric ground points through LiDAR data

analyse this compatibility, the 'a priori' (σ) and 'a posteriori' ($\hat{\sigma}$) altimetric accuracies were compared. This model was derived from the altimetric differences in the terrain between both datasets. To reject outliers from the corrected model, we eliminated the points whose altimetric difference fell outside the 95 % confidence interval (St-Onge et al. 2008).

DTM, DSM and CHM generation

After the registration of both datasets, the different digital models relating to terrain (DTM), surface (DSM) and canopy (CHM) were obtained by surface generation in the form of triangular meshes from the resulting classified cloud. These meshes had to be filtered and refined to remove the errors generated during the automated process.

This step used the approximation of Attene (2010), which incorporates several automated and sequential tasks:

- Filling of holes through algorithms of planar triangulations (Barequet and Sharir 1995) or more complex approaches based on interpolation of the radial basis function (Branch et al. 2006), the minimum distance (Dolenc and Makela 1993) and the measurement of angles (Bøhn and Wozny 1992; Varnuška et al. 2005).
- Repair of meshing gaps, based on minimum threshold distance algorithms (Rock and Wozny 1992; Barequet and Kumar 1997).
- Removal of topological noise, allowing the mesh to be re-triangulated locally (Guskov and Wood 2001).
- Removal of geometric noise by algorithms that apply filters as anti-aliased Laplacians in general or specific zones (Fan et al. 2008).

Finally, the CHM was obtained from the difference between the photogrammetrical DSM and the DTM resulting from the fusion of the point clouds (Järnstedt et al. 2012). The CHM represents the normalised heights of the vegetation with respect to the surface of the terrain, with a planimetric resolution of 1 m (D'Oliveira et al. 2012).

Experimental results

This study was conducted in an area of public land in the municipality of Bienservida in the province of Albacete (Spain). In particular, the study zone is located on land identified in the Public Usefulness Catalogue as No. 26. Figure 5a shows a map with the location of the study zone outlined in white. The scrubland area covers 1100 Ha. This is of great interest from a forestry perspective because the densely forested zone hosts a forest mass composed of *Pinus nigra* with different fractions of coverage according to the National Forest Inventory of Spain. The area also has a steep topography, and thus photogrammetric surveys are more appropriate from a practical point of view than classic forestry methods. The choice of this zone was also based on the availability of a pre-existing work plan that included the selected land and incorporated a classic forestry inventory. Thus, we established a zone of 2.00 km^2 (Fig. 5b) as the study area where we could apply the proposed methodology.

Regarding the LiDAR dataset, despite its official source, it was necessary to validate the data in advance by visual checking and manual refining. As a result, some outliers such as 'vegetation' or 'noise' were classified as 'ground', whereas some buildings were classified as 'vegetation'. To contrast changes in the LiDAR cloud with the initial classification, a confusion matrix was developed. A total of 4,822,511 points were classified correctly, obtaining a global accuracy of 99.98 %. An analysis of the confusion matrix, including the errors of commission and omission as well as producer and user accuracy can be seen in Table 3. These results show the insignificance of the incorrectly classified points in relation to the entirety of the cloud. A 1 % error was only exceeded by the 'others' class due to the presence of incorrect ground and vegetation points.

To perform photogrammetric data acquisition, the flight over the study area was planned with a height of 300 m, corresponding to a 7.50-cm GSD. The camera shooting interval was configured according to the minimum forward overlap and flight speed to meet the flight planning requirements and avoid image blurring, respectively (see "Flight planning and execution" section for more details). The obtained flight plan is outlined in Fig. 6, in which the rectangles represent the footprint of each image (area covered on the ground) resulting from each camera position (circles) along the flight strips. These footprints were

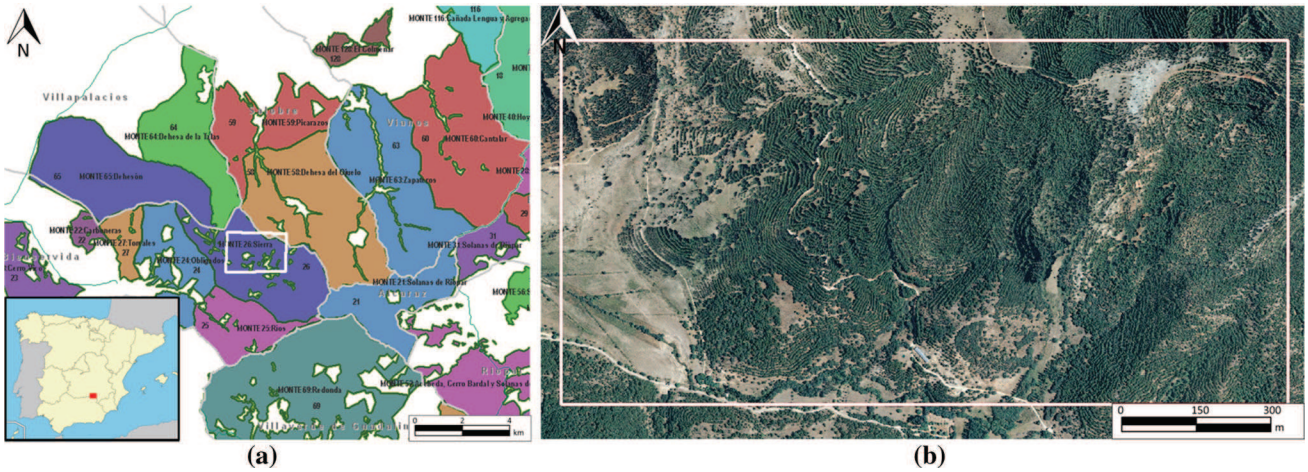

Fig. 5 **a** Location map with a box around the study area (*white rectangle*) and **b** orthophoto of the study area (EPSG code 25830)

Table 3 (a) Confusion matrix from the LiDAR data considering 'ground' and 'vegetation' classes and (b) errors of commission and omission and user and producer accuracy

	Refined LiDAR Data			
	Vegetation	Ground	Others	
(a)				
Initial LiDAR data				
Vegetation	3,674,535	0	325	3,674,860
Ground	517	1,145,807	20	1,146,344
Others	0	0	2169	2169
	3,675,052	1,145,807	2514	4,823,373
	Commission %	Omission %	Producer accuracy	User accuracy
(b)				
Vegetation	0.009	0.014	99.991	99.986
Ground	0.047	0.000	99.953	100.000
Others	0.000	13.723	100.000	86.277
	Global accuracy: 99.982 %			

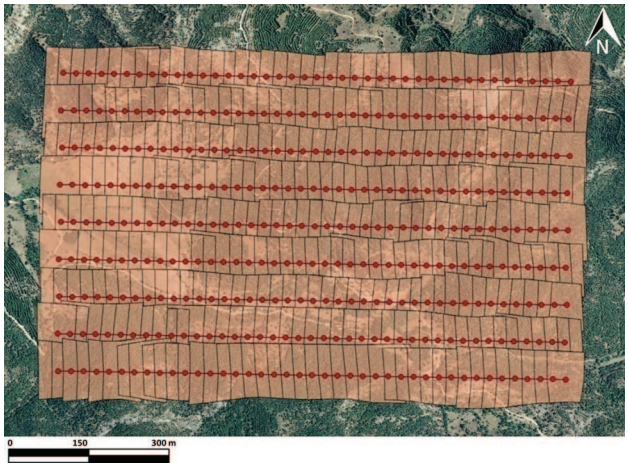

Fig. 6 Flight planning, 0.08 m GSD: *rectangles* represent the footprint of each image, and circles are the camera positions along the flight strips (EPSG code 25830)

projected based on the DTM ground relief to verify compliance with the flight parameter requirements.

The flight was carried out on 5 December 2013, covering a greater area than proposed to ensure total coverage of the study area. The flight run followed the established plan. Finally, images were georeferenced according to ETRS89 UTM 30 North (Coordinate Reference System, CRS EPSG code 25830), which is required by Spanish legislation for all geomatic products. The Albacete station was taken as a reference from the ERGNSS network (network of permanent geodetic GNSS stations of the National Geographic Institute of Spain) and used to correct the position of the RTK solution. In the navigation phase, which used a GNSS, WGS84 CRS was employed (EPSG code 4326). This georeferencing served as a preliminary photogrammetric adjustment and helped the process of computational matching.

Before the flight, 29 artificial ground points were placed in the zone to be measured by GNSS; these acted as control and check points. A georeferencing precision of 0.05 m was obtained in GNSS measurement post-processing.

In the conventional photogrammetric processing method carried out according to "Low-cost photogrammetric workflow" section, a total of 12,732,877 matching points were obtained, detecting 2,399,164 outliers through a robust estimation of the fundamental matrix (Barazzetti et al. 2010). The generated 3D dense model (Fig. 7) was composed of 290 million points after the processing of 1001 images, which is a density of 145 points/m^2. The model was georeferenced using 17 ground control points, obtaining an absolute georeferencing error of 1.21 m from the check points.

Once the photogrammetric point cloud had been generated, it was necessary to classify the points according to two classes: ground and vegetation. To distinguish the vegetation, radiometric segmentation was carried out, taking advantage of the visible spectrum of the photogrammetric point cloud. Figure 8 shows an example of the results of this processing.

Next, geometric segmentation was performed, working with the non-vegetation class, which was re-labelled 'ground'. The resulting photogrammetric point cloud classification is outlined in Table 4.

To analyse the statistical compatibility of both data sources (LiDAR and photogrammetry), the accuracies of both sets of registrations were compared. The 'a priori' accuracy was $\sigma = 0.41$ m (Eq. 2) while the 'a posteriori' accuracy obtained was $\hat{\sigma} = 0.47$ m, being the mean altimetric accuracy 0.17 m, confirming the validity of the results. These values were acquired in areas sharing common ground points between the LiDAR and refined photogrammetric point clouds, thus generating an altimetric difference map.

$$\sigma_{\text{fusion}} = \sqrt{(\sigma^2_{\text{photogrammetry}} + \sigma^2_{\text{LiDAR}})}$$

$$\sigma_{\text{fusion}} = \sqrt{(0.10^2 + 0.40^2)} = 0.41\,\text{m} \quad (2)$$

On the map of altimetric differences, we removed the values that fell outside a 95 % confidence interval, and the remaining differences were interpolated to obtain values at points lacking photogrammetric terrain data. Figure 9 shows a Q–Q plot of the map's height differences compared with standard normal quantiles, demonstrating a non-Gaussian distribution of the errors (absence of

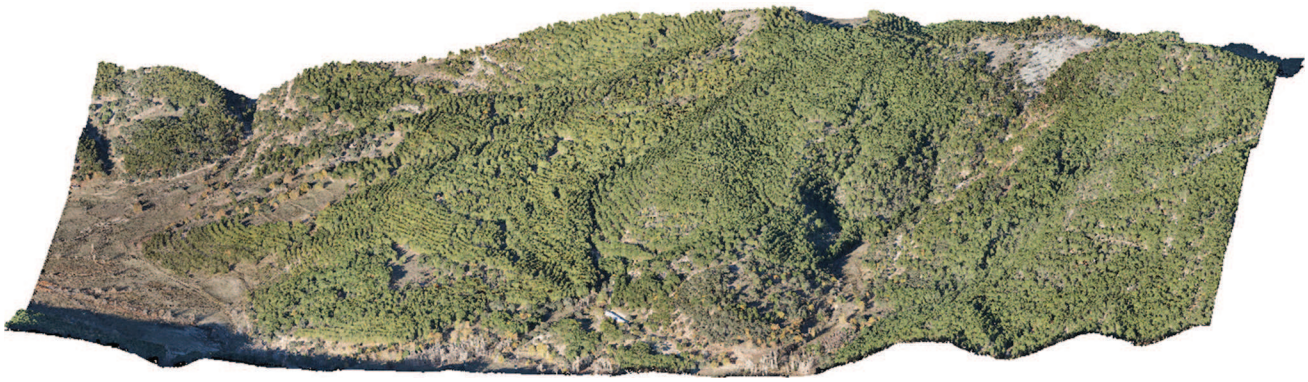

Fig. 7 Photogrammetric dense point cloud of the study area (145 points/m^2)

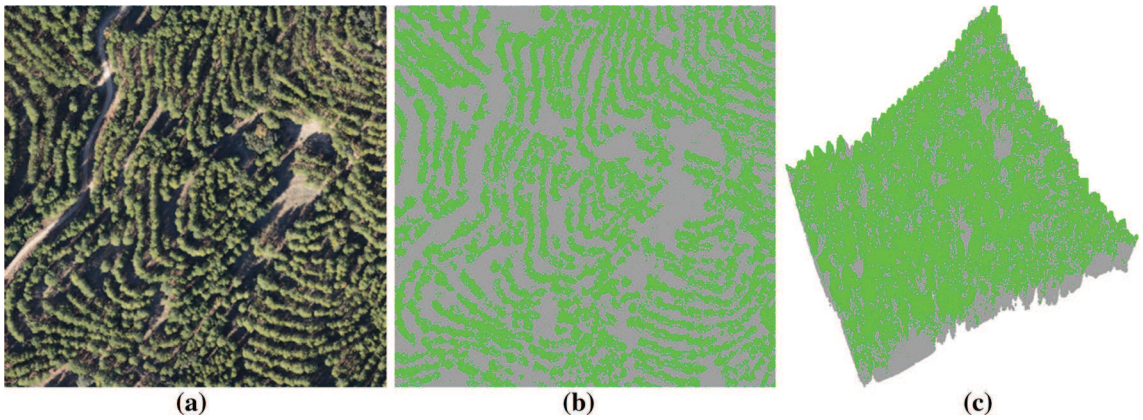

Fig. 8 Examples of radiometric segmentation of the photogrammetric point cloud. **a** Photogrammetric point cloud, **b** classified vegetation (*green*), **c** 3D classification view

Table 4 Classification of the photogrammetric cloud

Classification	No. points	%
Ground	29,281,752	17.70
Vegetation	135,562,812	81.92
Noise	528,961	0.32
Building	86,378	0.05
Wire conductor	12,668	0.01
Tower	2479	0.00

systematism), with some values that exceed the estimated accuracy. This is because the georeferencing of the LiDAR and photogrammetric data was not very rigorous owing to the scant topographic support of the LiDAR data, the automated matching processes, the use of low-accuracy inertial sensors and GNSS, and the use of non-metric cameras for the low-cost photogrammetry. Owing to this distribution, upon applying a solid-rigid transformation whose principal component is translation on the z axis, the error committed at certain points would be increased. Table 5 shows the map's statistical parameters and values.

In light of the above, we designed a discrete *correction model* (section "Fusion of point clouds") that improved the accuracy of the registration based on the altimetric differences map. The model was applied to LiDAR terrain data at points lacking photogrammetric information by means of a computer application designed for this end, as shown in Fig. 10. These corrected points were included in the photogrammetric point cloud, thus obtaining the fused point cloud.

Once both datasets had been fused, the properties of the final point cloud were analysed, checking for the absence of vegetation points with negative height. Table 6 shows the number of points belonging to each class together with the range of elevations and height normalised with respect to the ground class. Figure 11 shows the final point cloud for vegetation, ground and building classifications, seen in plan view.

As final results, Figs. 12, 13 and 14 show the Digital Terrain, Surface and Canopy Models obtained from the hybrid cloud, rasterised with a mesh size of 1 m.

After analysis of the CHM, we observed that there were very few cases in which the vegetation surpassed a height of 20 m. The *P. nigra* specimens in the zone were between 20 and 23 m in height. There was one case in which a

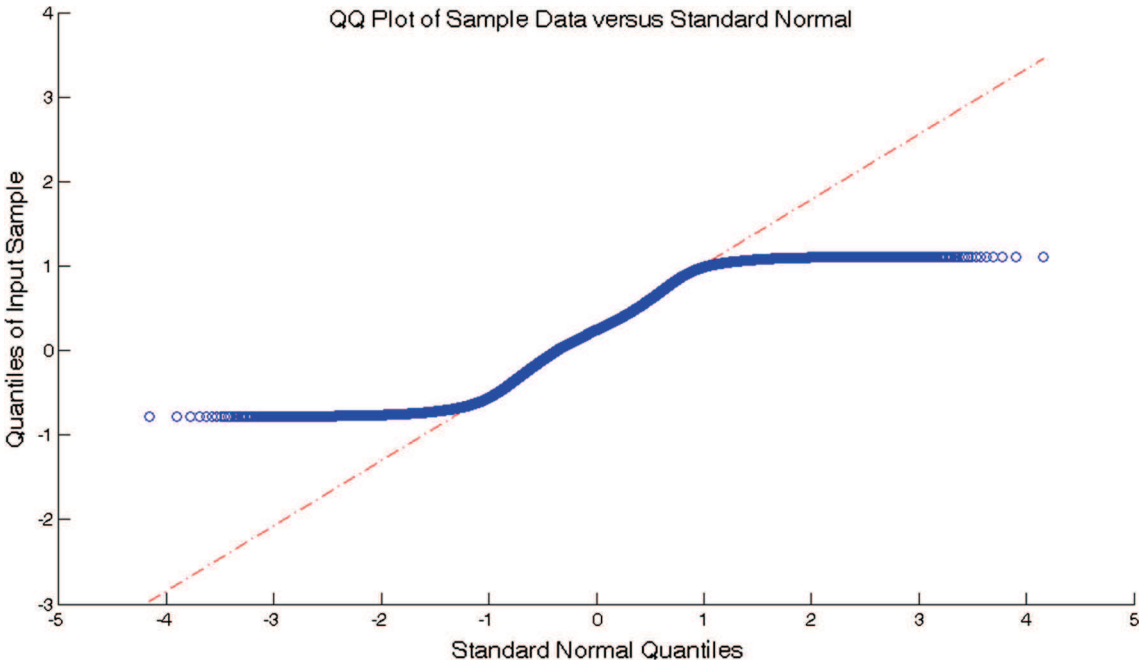

Fig. 9 Q–Q plot of the altimetric difference map versus standard normal quantiles

Table 5 Statistical data of the altimetric differences map

Maximum (m)	1.090
Mean (m)	0.226
Minimum (m)	−0.760
Std. deviation (m)	0.364

height of 27.7 m was attained, but this specimen was not a pine and was deciduous; it was probably a poplar, whose heights can reach 35 m.

The results allowed us to explore the development of forest growth in the area. To accomplish this, we analysed

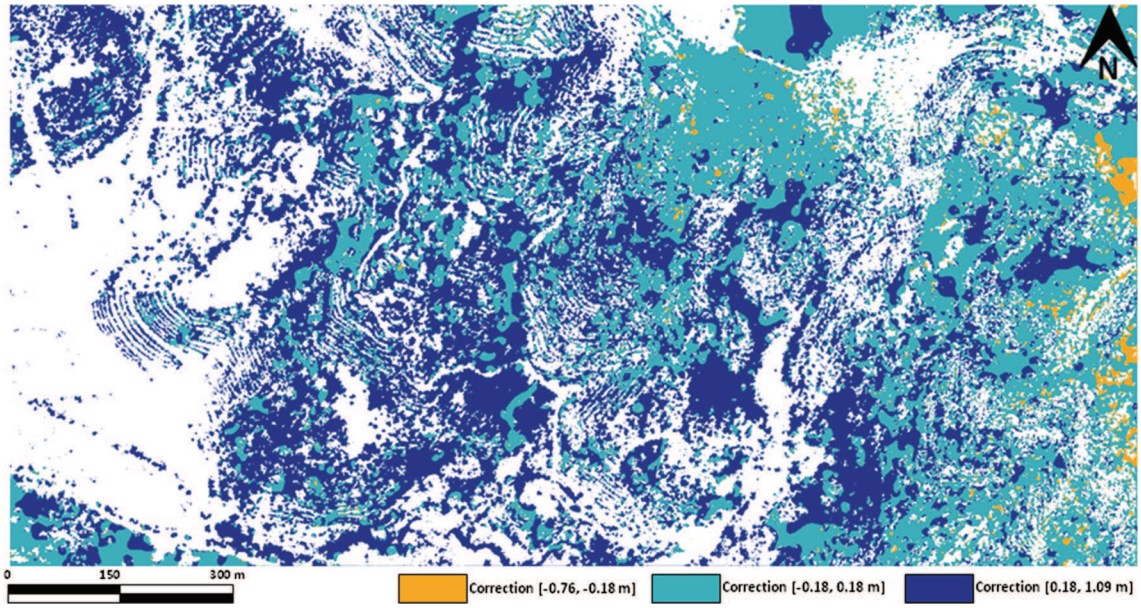

Fig. 10 Correction model coded by colour (EPSG code 25830)

Table 6 Classification of the final fusion cloud

Classification	No. points	%	Z_Min (m)	Z_Max (m)	Height (m)
Ground	29,220,875	17.78	1111.24	1406.59	0
Low vegetation	22,638,874	13.78	1111.50	1407.50	(0–1]
Medium vegetation	17,920,617	10.91	1112.68	1409.46	[1–3]
High vegetation	93,514,449	56.93	1113.50	1412.49	[3–27.67]
Building	86,378	0.05	1119.99	1184.34	–
Others	911,914	0.55	–	–	–

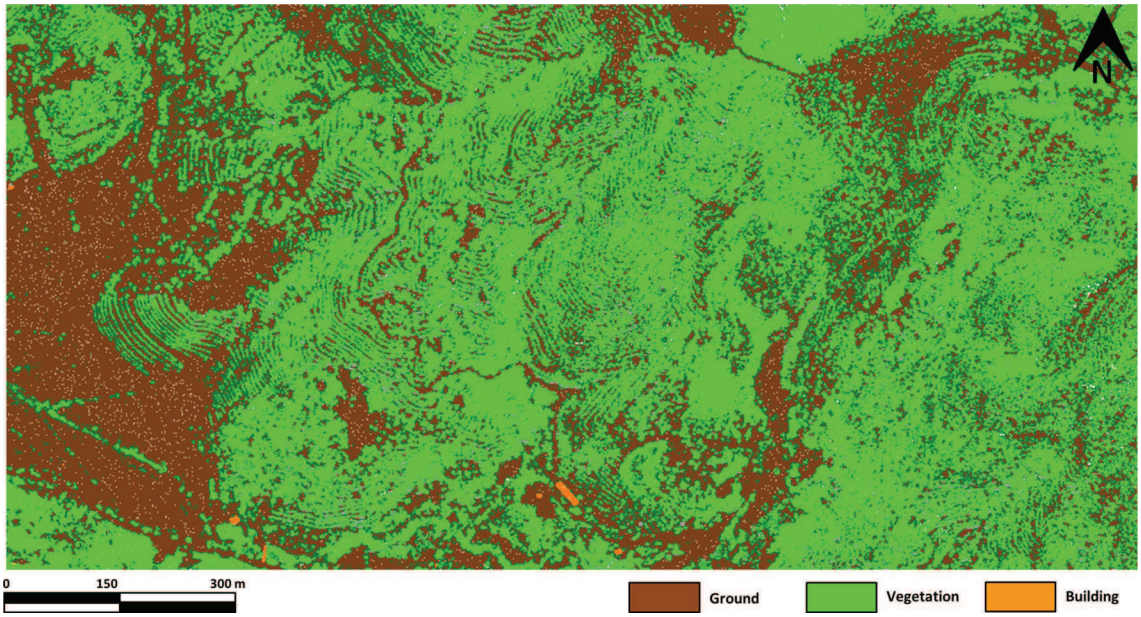

Fig. 11 Plan view of the final classified fusion cloud

Fig. 12 Digital terrain model

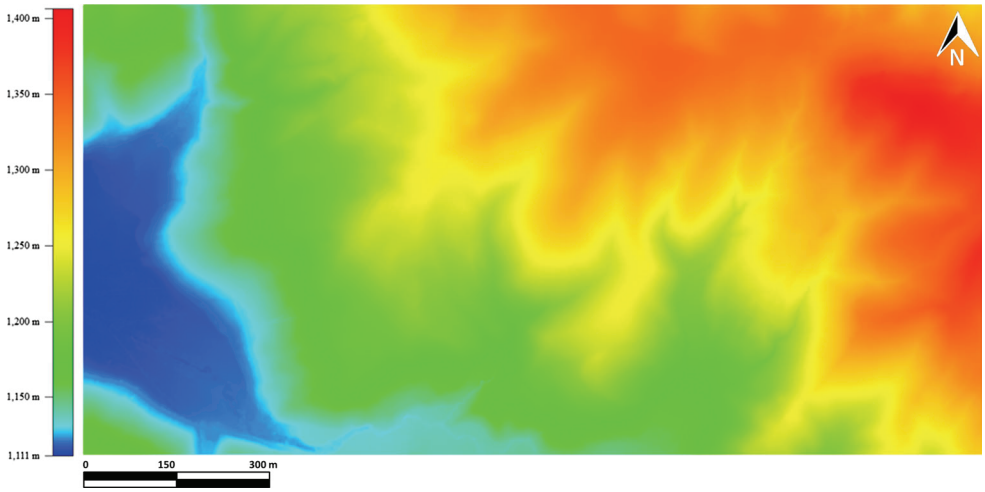

the distribution of the differences in plant volume between the CHM from the LiDAR data taken in 2009 and that generated from the hybrid point cloud in late 2013, both with respect to their respective DTMs. The increase in biomass volume that occurred during the interim was 3,318,501 m^3 in the 2.00 km^2 study area. This was due to the protectionist legislation enacted in the zone during those years (Cerro and Borja 2007).

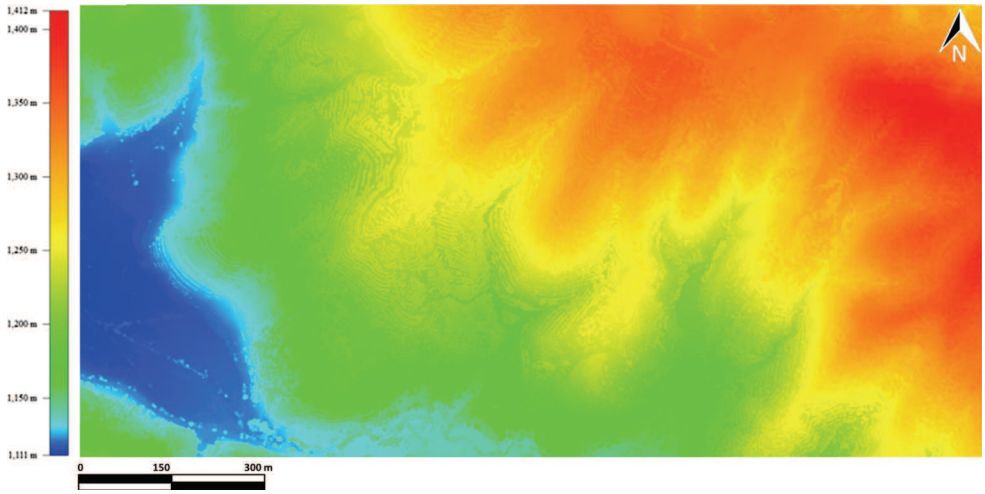

Fig. 13 Digital surface model

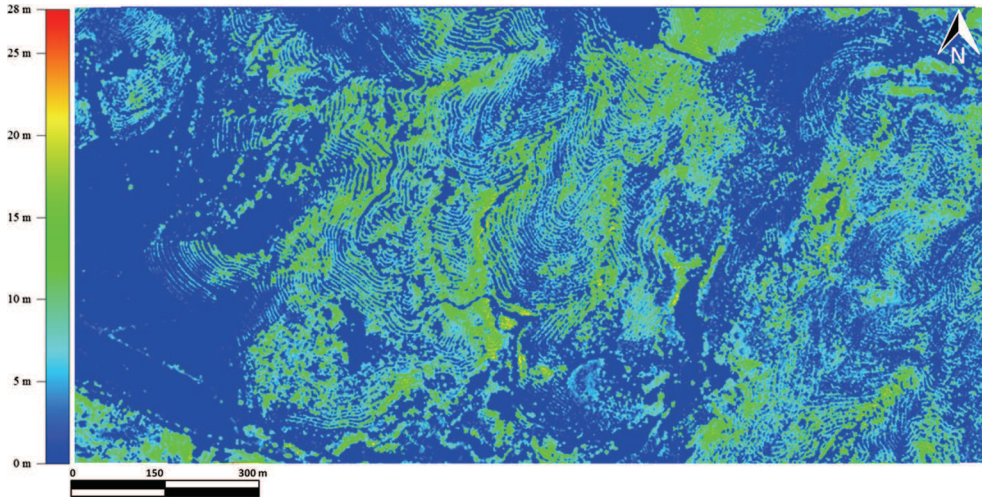

Fig. 14 Canopy height model

Conclusions

This paper describes a successful methodology that generates a Canopy Height Model for conducting forest inventories such a stratification of forest masses to forest management unit applications or a stock calculation and for fire studies obtaining combustible models. This CHM permits a better understanding of the forest structure in detail, allowing to know the relationships between the flora, the fauna and the soil over large extensions. The combined use of low-cost photogrammetry based on the use of economical, conventional, non-metric digital cameras and aerial LiDAR open data, together with the use of the latest computational vision techniques and geomatic tools, provides useful information for forestry applications.

In particular, by integrating the terrain data in the photogrammetric cloud, it is possible to incorporate LiDAR's capacity for terrain detection in zones of dense vegetation with the greater spatial, radiometric and temporal resolution of low-cost photogrammetry from alternative platforms such as the aerial trike or RPAS. Moreover, these platforms allow the loading of sensors suitable for vegetation analysis, depending on their payload capacity. Thus, it is possible to carry out a radiometric classification of the vegetation that improves upon current morphological methods. In this sense, we define a correction model that allows LiDAR data to be adjusted to the photogrammetric point cloud, obtaining an altimetric accuracy of 0.47 m for the registration data.

The advantage offered by this methodology is that it allows a CHM to be obtained with adequate phenological detail due to the combination of LiDAR flights performed at low temporal resolution and low-cost photogrammetric flights performed with the required periodicity. This also allows a reduction in the errors that arise in dasometric assessments upon incorporating models for the prediction of vegetation growth.

It is worth noting that the statistical compatibility of both sources of data could be improved in the data acquisition phase with appropriate field topographic support.

That is, photogrammetric point cloud georeferencing can be improved by designing pre-signalling targets of suitable colour for forestry applications and for later measurement in the images collected. It might even be possible to improve the targets' design to facilitate their detection and the automated extraction of the centroid. Another proposal would involve the incorporation of metric cameras, although in the case of RPAS this depends on the platform's payload capacity. This would increase both the associated cost and the accuracy.

The proposed methodology reduces the time required for acquisition and processing compared with that of traditional techniques of forest inventorying, with the added advantage that it provides vectorial information in the form of classified point clouds. This implies an increase in final accuracy at the rodal level and simplified integration and management of forestry information in Geographic Information Systems. At the same time, the subjectivity associated with operator-generated uncertainty is removed. Needless to say that the complementary of both techniques would offer to reach better results, taking advantages of the spatial continuity of the remote sensing in order to extrapolate the manual measurements of the trees.

In future work, we shall address the forestry variables in the obtained dense cloud and perform a comparative study with the variables obtained from the LiDAR information, applying rodal, individual-tree or even a combination of both methods to benefit from the high resolution of the initial data. To date, from the obtained CHM, essential tree parameters such as diameter at breast height (DBH) or distinguishing between species are not reliably derived yet. Another line of enquiry will be to contrast the variables obtained from the dense cloud with other data from a classic inventory of the study zone, i.e., the National Forest Inventory of Spain and the inventory drafted by the Public Land and Natural Spaces Service of the Agricultural Commission of the Regional Government of Castilla-La Mancha, Spain.

Author contribution statement B.F.-G., D.H.-L. and D.G.-A. planned the experiment and supervised processing, M.H.-H., B.F.-G. and S.B.-L. performed the study, analysed data and prepared the manuscript and P.R.-G. contributed to data interpretation. All authors wrote the manuscript.

Acknowledgments This research arose as a pilot project in collaboration with the Public Land and Natural Spaces Service, belonging to the Peripheral Services of the Agricultural Commission of the Regional Government of Castilla-La Mancha; the Institute for Development of the University of Castilla-La Mancha; the Forestry and Natural Spaces Service; the Agriculture, Environment and Rural Development Department of the Castilla-La Mancha Regional Government; and the USAL research group Geomatic Technologies for the 3D digitalisation and modelling of complex objects (TIDOP).

Compliance with ethical standards

Conflict of interest The authors declare that they have no conflict of interest.

References

ASPRS Foundation (2012) LASer (LAS) file format exchange activities. http://www.asprs.org/Committee-General/LASer-LAS-File-Format-Exchange-Activities.html. Accessed 01 Nov 2014

Attene M (2010) A lightweight approach to repairing digitized polygon meshes. Vis Comput 26(11):1393–1406

Axelsson P (1999) Processing of laser scanner data—algorithms and applications. ISPRS J Photogramm Remote Sens 54(2):138–147

Barazzetti L, Remondino F, Scaioni M, Brumana R (2010) Fully automatic UAV image-based sensor orientation. In: Proceedings of the 2010 Canadian geomatics conference and symposium of commission I

Barequet G, Kumar S (1997) Repairing CAD models. In: Visualization'97, proceedings, pp 363–370. IEEE

Barequet G, Sharir M (1995) Filling gaps in the boundary of a polyhedron. Comput Aided Geom Des 12(2):207–229

Benko M, Balenovic I (2011) Past, present and future of application of remote sensing methods in croatian forest inventory. Sumarski List 135:272–281

Bohlin J, Wallerman J, Fransson JES (2012) Forest variable estimation using photogrammetric matching of digital aerial images in combination with a high-resolution DEM. Scand J For Res 27(7):692–699

Bøhn JH, Wozny MJ (1992) Automatic CAD-model repair: shell-closure. In: Proceedings of symposium on solid freeform fabrication, pp 86–94

Branch D, Dang LC, Hall N, Ketchum W, Melakayil M, Parrent J, Baron E (2006) Comparative direct analysis of type Ia supernova spectra. II. Maximum light. Publ Astron Soc Pac 118(842):560–571

Cerro A, Borja MEL (2007) El "Pinus nigra arn." en la Serranía de Cuenca: estudio sobre su regeneración natural y bases para su gestión. Junta de Comunidades de Castilla-La Mancha, Dirección General del Medio Ambiente

Chauve A, Mallet C, Bretar F, Durrieu S, Deseilligny MP, Puech W (2007) Processing full-waveform lidar data: modelling raw signals. In: International archives of photogrammetry, remote sensing and spatial information sciences, pp 102–107

CNIG (National Center of Geographic Information in Spain) (2009) Technical specifications for the National Plan of Aerial Orthophotography (PNOA). ftp://pnoa.ign.es. Accessed 01 Nov 2014

CNIG (National Center of Geographic Information in Spain) (2015). http://centrodedescargas.cnig.es/CentroDescargas/. Accessed 16 July 2015

Dolenc A, Makela I (1993) Some efficient procedures for correcting triangulated models. In: Proceedings of solid freeform fabrication symposium, pp 126–134

D'Oliveira MV, Reutebuch SE, McGaughey RJ, Andersen HE (2012) Estimating forest biomass and identifying low-intensity logging areas using airborne scanning lidar in Antimary State Forest, Acre State, Western Brazilian Amazon. Remote Sens Environ 124:479–491

Eid T, Gobakken T, Naesset E (2004) Comparing stand inventories for large areas based on photo-interpretation and laser scanning by means of cost-plus-loss analyses. Scand J For Res 19(6):512–523

Estornell J, Ruiz LA, Velazquez-Marti B, Hermosilla T (2012) Assessment of factors affecting shrub volume estimations using airborne discrete-return LiDAR data in Mediterranean areas. J Appl Remote Sens 6(1):063544

Fan YZ, Tam BS, Zhou J (2008) Maximizing spectral radius of unoriented Laplacian matrix over bicyclic graphs of a given order. Linear Multilinear Algebra 56(4):381–397

Gleason CJ, Im J (2012) Forest biomass estimation from airborne LiDAR data using machine learning approaches. Remote Sens Environ 125:80–91

Gonzalez E, Dieguez U, Miranda D (2012) Estimation of stand variables in Pinus radiata D. Don plantations using different LiDAR pulse densities. Forestry 85(2):281–292

González-Aguilera D, Guerrero D, Hernández-López D, Rodríguez-Gonzálvez P, Pierrot M, Fernández-Hernández J (2013) PW, photogrammetry workbench

González-Ferreiro E, Diéguez-Aranda U, Crecente-Campo F, Barreiro-Fernández L, Miranda D, Castedo-Dorado F (2014) Modelling canopy fuel variables for Pinus radiata D. Don in NW Spain with low-density LiDAR data. Int J Wildl Fire 23(3):350–362

Gupta S, Weinacker H, Koch B (2010) Comparative analysis of clustering-based approaches for 3-D single tree detection using airborne fullwave lidar data. Remote Sens 2(4):968–989

Guskov I, Wood ZJ (2001) Topological noise removal. In: 2001 graphics interface proceedings, Ottawa, Canada, 19

Hernández-Lopez D, Felipe B, González D, Arias B (2013) An automatic approach to UAV flight planning and control for photogrammetric applications: a test case in the Asturias Region (Spain). Photogramm Eng Remote Sens 79(1):87–98

Hyyppä J, Hyyppä H, Leckie D, Gougeon F, Yu X, Maltamo M (2008) Review of methods of small-footprint airborne laser scanning for extracting forest inventory data in boreal forests. Int J Remote Sens 29(5):1339–1366

IGN (2015) http://pnoa.ign.es/presentacion. Accessed 16 July 2015

Jaakkola A, Hyyppä J, Kukko A, Yu X, Kaartinen H, Lehtomäki M, Lin Y (2010) A low-cost multi-sensoral mobile mapping system and its feasibility for tree measurements. ISPRS J Photogramm Remote Sens 65:514–522

Järnstedt J, Pekkarinen A, Tuominen S, Ginzler C, Holopainen M, Viitala R (2012) Forest variable estimation using a high-resolution digital surface model. ISPRS J Photogramm Remote Sens 74:78–84

Kankare V, Vastaranta M, Holopainen M, Räty M, Yu X, Hyyppä J, Viitala R (2013) Retrieval of forest aboveground biomass and stem volume with airborne scanning LiDAR. Remote Sens 5(5):2257–2274

Kohavi R, Provost F (1998) Glossary of terms. Mach Learn 30(2–3):271–274

Kraus K (2007) Photogrammetry, 2007. Geometry from images and laser scans. Walter de Gruyter

Lim KS, Treitz PM (2004) Estimation of above ground forest biomass from airborne discrete return laser scanner data using canopy-based quantile estimators. Scand J For Res 19(6):558–570

Lisein J, Pierrot M, Bonnet S, Lejeune P (2013) A photogrammetric workflow for the creation of a forest canopy height model from small unmanned aerial system imagery. Forests 4(4):922–944

Lowe DG (2004) Distinctive image features from scale-invariant keypoints. Int J Comput Vis 60:91–110

Magnussen S, Boudewyn P, Wulder MA, Seemann D (2000) Predictions of forest inventory cover type proportions using landsat TM. Silva Fennica 34(4):351–370

Magnussen S, Naesset E, Wulder MA (2007) Efficient multiresolution spatial predictions for large data arrays. Remote Sens Environ 109(4):451–463

Magnusson M, Fransson JES, Olsson H (2007) Aerial photo-interpretation using Z/I DMC images for estimation of forest variables. Scand J For Res 22(3):254–266

Mallet C, Bretar F (2009) Full-waveform topographic lidar: state-of-the-art. ISPRS J Photogramm Remote Sens 64(1):1–16

Means JE, Acker SA, Fitt BJ, Renslow M, Emerson L, Hendrix CJ (2000) Predicting forest stand characteristics with airborne scanning lidar. Photogramm Eng Remote Sens 66(11):1367–1372

Mora B, Wulder MA, Hobart GW, White JC, Bater CW, Gougeon FA, Coops NC (2013) Forest inventory stand height estimates from very high spatial resolution satellite imagery calibrated with lidar plots. Int J Remote Sens 34(12):4406–4424

Naesset E (1997) Estimating timber volume of forest stands using airborne laser scanner data. Remote Sens Environ 61(2):246–253

Naesset E (2004) Practical large-scale forest stand inventory using a small-footprint airborne scanning laser. Scand J For Res 19(2):164–179

Naesset E, Bollandsas OM, Gobakken T (2005) Comparing regression methods in estimation of biophysical properties of forest stands from two different inventories using laser scanner data. Remote Sens Environ 94(4):541–553

Navarro-Cerrillo RM, del Campo AD, Ceacero CJ, Quero JL, Hermoso de Mena J (2014) On the importance of topography, site quality, stock quality and planting date in a semiarid plantation: feasibility of using low-density LiDAR. Ecol Eng 67:25–38

NavCen (2008) Global positioning system standard positioning service performance standar, 4th edn. US Department of Defense: Position, Navigation and Timing Executive Committee, Washington

Nelson R, Krabill W, Tonelli J (1988) Estimating forest biomass and volume using airborne laser data. Remote Sens Environ 24(2):247–267

Nelson R, Oderwald R, Gregoire TG (1997) Separating the ground and airborne laser sampling phases to estimate tropical forest basal area, volume, and biomass. Remote Sens Environ 60(3):311–326

Nelson R, Parker G, Hom M (2003) A portable airborne laser system for forest inventory. Photogramm Eng Remote Sens 69(3):267–273

Ortega-Terol D, Moreno MA, Hernández-López D, Rodríguez-Gonzálvez P (2014) Survey and classification of large woody debris (LWD) in streams using generated low-cost geomatic products. Remote Sens 6:11770–11790

Pierrot-Deseilligny M, Clery I (2011) An open source bundle adjustment software for automatic calibration and orientation of set of images. In: Apero, ISPRS symposium, 3DARCH11, Trento, Italy, March 2–4, pp 269–276

Popescu SC, Wynne RH, Nelson RF (2002) Estimating plot-level tree heights with lidar: local filtering with a canopy-height based variable window size. Comput Electron Agric 37(1):71–95

Premerlani W, Bizard P (2014) Direction cosine matrix IMU: theory. http://gentlenav.googlecode.com/files/DCMDraft2.pdf. Accessed 20 Dec 2014

Richardson JJ, Moskal LM (2011) Strengths and limitations of assessing forest density and spatial configuration with aerial LiDAR. Remote Sens Environ 115(10):2640–2651

Rock SJ, Wozny MJ (1992) Generating topological information from a bucket of facets. In: Solid freeform fabrication symposium proceedings, pp 251–259. The University of Texas at Austin, Austin

St-Onge B, Vega C, Fournier RA, Hu Y (2008) Mapping canopy height using a combination of digital stereo-photogrammetry and lidar. Int J Remote Sens 29(11):3343–3364

Takasu T (2009) RTKLIB: open source program package for RTK-GPS. FOSS4G, Tokyo, Japan

Tao W, Lei Y, Mooney P (2011) Dense point cloud extraction from UAV captured images in forest area. In: Proceedings of the 2011 IEEE international conference on spatial data mining and geographical knowledge services (ICSDM), pp 389–392

Varnuška M, Parus J, Kolingerová I (2005) Simple holes triangulation in surface reconstruction. In: Proceedings of ALGORITMY, pp 280–289

Wallace L, Lucieer A, Watson C, Turner D (2012) Development of a UAV-LiDAR system with application to forest inventory. Remote Sens 4:1519–1543

Wang Z, Boesch R, Ginzler C (2007) Color and lidar data fusion: application to automatic forest boundary delineation in aerial images. Int Arch Photogramm Remote Sens Spat Inf Sci [CD] 36(1):W51

Weinacker H, Koch B, Heyder U, Weinacker R (2004) Development of filtering, segmentation and modelling modules for lidar and multispectral data as a fundament of an automatic forest inventory system. Int Arch Photogramm Remote Sens Spat Inf Sci 36(Part 8):50–55

White JC, Wulder MA, Varhola A, Vastaranta M, Coops NC, Cook BD, Woods M (2013a) A best practices guide for generating forest inventory attributes from airborne laser scanning data using an area-based approach. For Chron 89(6):722–723

White JC, Wulder MA, Vastaranta M, Coops NC, Pitt D, Woods M (2013b) The utility of image-based point clouds for forest inventory: a comparison with airborne laser scanning. Forests 4(3):518–536

Willers JL, Wu J, O'Hara C, Jenkins JN (2012) A categorical, improper probability method for combining NDVI and LiDAR elevation information for potential cotton precision agricultural applications. Comput Electron Agric 82:15–22

Wulder MA, White JC, Fournier RA, Luther JE, Magnussen S (2008a) Spatially explicit large area biomass estimation: three approaches using forest inventory and remotely sensed imagery in a GIS. Sensors 8(1):529–560

Wulder MA, White JC, Hay GJ, Castilla G (2008b) Towards automated segmentation of forest inventory polygons on high spatial resolution satellite imagery. For Chron 84(2):221–230

Wulder MA, White JC, Nelson RF, Næsset E, Ørka HO, Coops NC, Gobakken T (2012) Lidar sampling for large-area forest characterization: a review. Remote Sens Environ 121:196–209

Wulder MA, Coops NC, Hudak AT, Morsdorf F, Nelson R, Newnham G, Vastaranta M (2013) Status and prospects for LiDAR remote sensing of forested ecosystems. Can J Remote Sens 39(-sup1):S1–S5